ELSEVIER

Contents lists available at ScienceDirect

Applied Soft Computing

journal homepage: www.elsevier.com/locate/asoc





Fault analysis in clustered microgrids utilizing SVM-CNN and differential protection

Paul Arévalo ^{a,b}, Antonio Cano ^b, Darío Benavides ^b, Francisco Jurado ^{b,*}

- a Department of Electrical Engineering. Electronics and Telecommunications (DEET). University of Cuenca. 010107 Balzay Campus. Cuenca.Azuay. Ecuador
- ^b Department of Electrical Engineering, University of Jaen, Jaén, Spain

HIGHLIGHTS

- DG and RES integration in modern grids and MGs enhances resilience but challenges fault detection due to low fault currents.
- Novel SVM-CNN methodology proposed for fault detection, addressing challenges like HIF detection.
- Proposed SVM-CNN achieves up to 100 % accuracy in fault detection, including HIF and islanding events.
- Results highlight methodology's effectiveness in improving fault response time and accuracy.

ARTICLE INFO

Keywords: Microgrids Renewable energy sources Fault detection Differential protection

ABSTRACT

The integration of distributed generation, microgrids, and renewable energy sources has significantly enhanced the resilience of modern electrical grids. However, this transition presents challenges in control, stability, safety, and protection due to low fault currents from renewables. This paper addresses these challenges by proposing novel methodologies to enhance fault detection, classification, and localization in microgrids. The literature review highlights a shift towards intelligent learning methods in microgrid protection systems, improving fault response times and identifying electrical faults, including high impedance faults. Nonetheless, existing methods often neglect high impedance fault detection and the integration of differential protection in clustered microgrids. To fill these gaps, this study presents a methodology combining support vector machines and convolutional neural networks for fault detection in microgrids, integrating differential protection for high impedance fault detection. The paper also proposes approaches to optimize protection in clustered microgrid systems. The effectiveness of the methodology is validated using Opal-RT through comparative analyses of signal decomposition techniques, performance and accuracy of support vector machines and convolutional neural networks, K-Fold validation, and sensitivity analysis. Results demonstrate robustness and high performance, achieving up to 100 % accuracy in fault detection and classification.

1. Introduction

The distributed generation (DG) is experiencing steady growth in modern electrical systems and smart grids, suggesting its integration with microgrid (MG) and renewable energy sources (RES). This transition process significantly enhances resilience in electrical grids [1,2]. The physical and coordinated integration of multiple MG groups into the electrical system enables improvement in distribution systems in terms of economy, resilience, and reliability [3,4]. Control strategies have been implemented to enhance stability and active damping, along with nonlinear control algorithms in microgrid cluster (MGC) [5], in addition

to coordinated distributed control based on multi-agent systems [6]. However, these changes during the transition pose challenges in control, stability, safety, and especially protection for current distribution electrical systems due to the low fault current provided by RES. This phenomenon poses a challenge for fault detection using conventional protection systems, necessitating the development of new techniques capable of identifying, locating, and classifying faults more effectively, whether internal or external to an MGC connected to an external grid. This paper focuses on addressing this issue.

In the literature review, there is an evolution in protection methods observed, ranging from simple analog relays to the latest advances and

E-mail address: fjurado@ujaen.es (F. Jurado).

https://doi.org/10.1016/j.asoc.2024.112031

Received 19 April 2024; Received in revised form 17 June 2024; Accepted 10 July 2024 Available online 19 July 2024

 $^{^{\}ast}$ Corresponding author.

trends in protection systems in MGs, which focus on intelligent learning methods [7]. These latter methods have improved fault response time, as indicated by some authors in [8]. Identification and location of electrical faults in renewable systems have also been enhanced, as described in [9,10], and the classification of different types of faults has been extensively studied in [9-12]. Detecting high impedance faults (HIF) presents a unique challenge for protecting distributed generation systems. Conventional techniques struggle to interpret HIF due to the low level of fault current involved [13], which can resemble other occurrences like line openings and closings. Therefore, accurately identifying, classifying, and locating a set of faults remains a significant challenge in MGCs, as highlighted by various researchers in this field [14]. On the other hand, quick fault clearance times are essential to prevent electrical system instability, with current relays aiming for times less than 50 ms [15]. Recently, researchers have developed techniques for detecting, classifying, and locating electrical faults involving the integration of artificial neural networks (ANN), machine learning (ML), or genetic algorithms (GA) applied to MG. The authors in [8], examines the coordination of directional overcurrent relays in MGs based on hybrid algorithms of heuristic-linear programming. On the other hand, another study has been presented with advanced methods based on ANN such as transfer learning technique for faults in transmission lines [16]. These have provided benefits in optimizing execution times and high accuracy. Deep convolutional neural network (ConvNet) has also been considered for fault detection, classification, identification, and location for MGs integrating PV systems in island mode [17]. Authors in [18] also propose a novel fault detection algorithm based on ANN and discrete Wavelet transform (DWT). This has allowed for increased reliability, improved system robustness, and detection in short time intervals in MGs [19]. Authors, based on the results of these studies validated with real-time simulation using RX62T with OP5600, conclude that the DWT technique is superior to the Fourier transform and the continuous Wavelet transform (WT) from the perspective of accuracy and simplicity.

Other studies propose the combination of principal component analysis of ANN and radial basis function neural network (RBFNN) for fault detection using differential protection in power transformers [20], where the authors manage to generate a trigger signal within 15 ms after the occurrence of the fault. Meanwhile, the authors in [21], present a new combination based on variational mode decomposition (VMD) and Hilbert transform (HT) as tools for differential protection in MGs [21]. The proposed system has been validated in real-time simulator OPAL-RT (optimized power system real-time) with the capability of detecting high impedance faults. Similarly, authors in [22] propose a novel method based on DWT with high performance speed and low sampling frequency. The results have been discussed with other existing methods for both grid-connected and islanded scenarios. Also, the Wavelet energy entropy ratio criterion is utilized for fault detection in electrical systems [23].

The combination of methods with HT has generated significant contributions in DC-MG protection. For example, in [24], the authors study the combination of VMD and HT for detecting the Wavelet components of DC perturbative signals. Additionally, HT has been used accurately in harmonic/interharmonic detection and monitoring techniques, fault detection, and diagnosis in synchronous motors. Furthermore, WT has also aroused great interest in the field of electrical protections in MGs, where methods for ground fault identification and fault detection and localization using different Wavelet approaches have been proposed. Likewise, the DWT has been studied for detecting faults in MGs, offering the advantage of stable protection under typical disturbances without fault. Other applications include high-frequency component extraction using DWT and its use in differential protection for internal faults, allowing real-time application with low computational effort. Additionally, strategies such as frequency-based current differential protection for distribution lines have been proposed, implementing digital signal processing to achieve fast response times.

The comprehensive review of literature reveals convergence with the present study in several critical aspects related to fault detection and protection in MGs [25]. Recent research has significantly advanced the application of techniques such as ANN, convolutional neural network (CNN), and DWT to enhance accuracy and efficiency in fault detection in MGs [8], [16], [18]. These approaches have proven effective in controlled environments but show a notable lack of attention towards HIF, which are crucial in distributed generation systems where fault current levels are low [26]. One critical gap identified in the literature is the insufficient integration of advanced protection techniques, such as differential protection, in MGC. While innovative schemes combining WT with data mining models have been proposed to enhance protection relay accuracy [27], these methods have not been widely implemented in MGC. This is due to the complexity of adapting these models to dynamic environments and the need for extensive validation under varying operational conditions.

Furthermore, while studies like that proposed by [28] have introduced deep learning models such as CNN transformers for fault detection and localization in distribution systems, there remains a continuous need to develop more effective methodologies to optimize protection in MGs, especially in complex clustered and interconnected environments. These models have shown significant improvements in fault type classification and location identification but must still address challenges such as adaptability to diverse MG topologies and robustness against changing operational conditions. Lastly, studies [29] and [26] emphasize the importance of integrating advanced techniques, such as CNNs optimized with optimization algorithms, to enhance accuracy and reliability in fault detection in MGs. These studies underscore the need to address the lack of scalable and adaptive methods capable of effectively handling fault detection in MGs with multiple distributed generation sources and significant operational variations.

Therefore, despite advancements in deep learning techniques for fault detection in MGs, there remains a lack of in-depth research on fully leveraging these differential characteristics. Current studies, [27] - [26] have explored various methodologies but have not effectively integrated differential protection with artificial intelligence techniques to maximize sensitivity and precision in detecting HIF and other subtle fault types. It is crucial to explore how differential protection can complement modern fault detection techniques. This integration could pave the way for improving efficiency and accuracy in clustered MG protection. By combining these methodologies, false alarms could be reduced, response times enhanced, and overall MG operation optimized, thereby providing more robust and adaptable protection.

In response to the gaps identified in the existing literature, this study offers several contributions to the field of fault detection, classification, and localization in MGC environments. It particularly focuses on challenges such as HIF, events, and the integration of differential protection. A methodology is proposed that combines SVM (support vector machine)-CNN for fault detection in MGs, adapting and applying this combination to enhance the accuracy and efficiency of fault identification in MGs, considering the variability of renewable resources and the low fault current they entail. Although these techniques have been previously explored in other contexts [29], [26], [30], their specific implementation in MGC, along with differential protection, is justified by their ability to overcome current limitations by integrating key differential characteristics. This concept addresses the challenges of conventional protections against events occurring inside or outside the MG cluster.

The importance of the proposed methodology for HIF, which do not produce current spikes but rather waveform deformation, is evident. This strategy leverages the capability of differential protection to sum or subtract current signals between different points of the network, allowing the detection of even the weakest fault currents masked by other events [26]. SVM is notable for its ability to effectively handle small and imbalanced datasets, utilizing optimal separation margins between classes for precise classifications. On the other hand, CNN is

recognized for its capacity to automatically learn and extract complex features from signals, such as those generated by electrical currents in MG systems. By combining SVM and CNN, the system's ability to detect, classify, and locate faults that are difficult to identify is significantly enhanced.

The study also presents real-time simulations using OPAL-RT to validate the computational simulations of the proposed method in real environments, including noise and time delays. In summary, the main contributions of this study include:

- Integration of SVM-CNN with DWT for precise fault detection and rapid classification and localization using a differential protection relay in a clustered MG environment.
- Evaluation of DWT, WPT, and VMD combined with the HT to optimize fault detection.
- Optimization of SVM-CNN hyperparameters to minimize the response time of the differential relay.

Therefore, this article is organized as follows: Section 2 examines the methodology of the paper, Section 3 presents the proposed method, while Section 4 elucidates the case study where the method is tested. Subsequently, Section 5 showcases the results, and the paper concludes in Section 6.

2. Methodology

The proposed methodology for fault detection in MGC is shown in Fig. 1. Fault current waveforms in different zones of the MG group are generated through simulations conducted in DIgSILENT PowerFactory software. These waveforms represent the current difference between two terminals of a transmission line, like what a differential protection system does. Subsequently, using a combination of SVM and CNN, fault detection, classification, and localization are performed within the MGC. The main objective of this SVM and CNN combination is to identify patterns enabling the detection of fault types, phases, and locations within the MGC. Additionally, it has been extended to include the detection of HIF, line opening and closing events, and isolation scenarios.

To evaluate the effectiveness of the proposed methodology, detailed

comparisons are conducted between the Wavelet approximation coefficient (WAC) under normal operating conditions, serving as a baseline reference. Specifically, it is compared with decomposition using the Wavelet packet transform (WPT) and the VMD combined with the HT, revealing up to 20 intrinsic mode functions (IMF). This analysis is conducted with the aim of identifying the most prominent coefficients in simulated fault scenarios, specifically during a single-phase ground fault. This analysis aims to identify the most prominent coefficients in simulated fault scenarios, particularly during single-phase ground faults. The objective is to improve fault detection capabilities while varying the fault resistance. In this context, preference is given to DWT approximation coefficients due to their ability to effectively highlight and classify faults, especially in the presence of high fault resistances. Finally, OPAL-RT is utilized to validate the method in real-time scenarios, ensuring its practical applicability.

2.1. Mathematical modeling of DWT

The DWT is a highly utilized mathematical function owing to its wide window breadth in the time domain, rendering it particularly intriguing for the study of transient signals. The WT undertakes the process of treating the selected wavelet and the signal x(t), where represents the measured waveform. The calculation process of WT is expressed as follows with Eq. (1) [15]:

$$X(\omega|a,b) = \frac{1}{\sqrt{a}} \int_{-\infty}^{\infty} x(t) \psi^* \left(\frac{t-b}{a}\right) dt \tag{1}$$

where a is the scale factor and b is the temporal shift, $\psi(t)$ is the chosen wavelet mother, ψ is the complex conjugate of the wavelet. For values of a and b, $\psi\left(\frac{t-b}{a}\right)$ yields the daughter of $\psi(t)$, where the value of a is determined by the pseudo-frequency [31]. For discrete-time signals, DWT decomposes the signal using wavelet functions $\psi(t)$. This process involves applying discrete filters $c_o(k)$ and dj(k) for the DWT calculation. The signal f(t) can be expressed with Eq. (2) [31]:

$$f(t) = \sum_{k} c_0(k)\phi(2^{j}t - k) + \sum_{k}\sum_{j=1} d_j(k)\varphi(2^{j}t - k)$$
 (2)

According to Parseval's theorem [32], the Wavelet entropy is

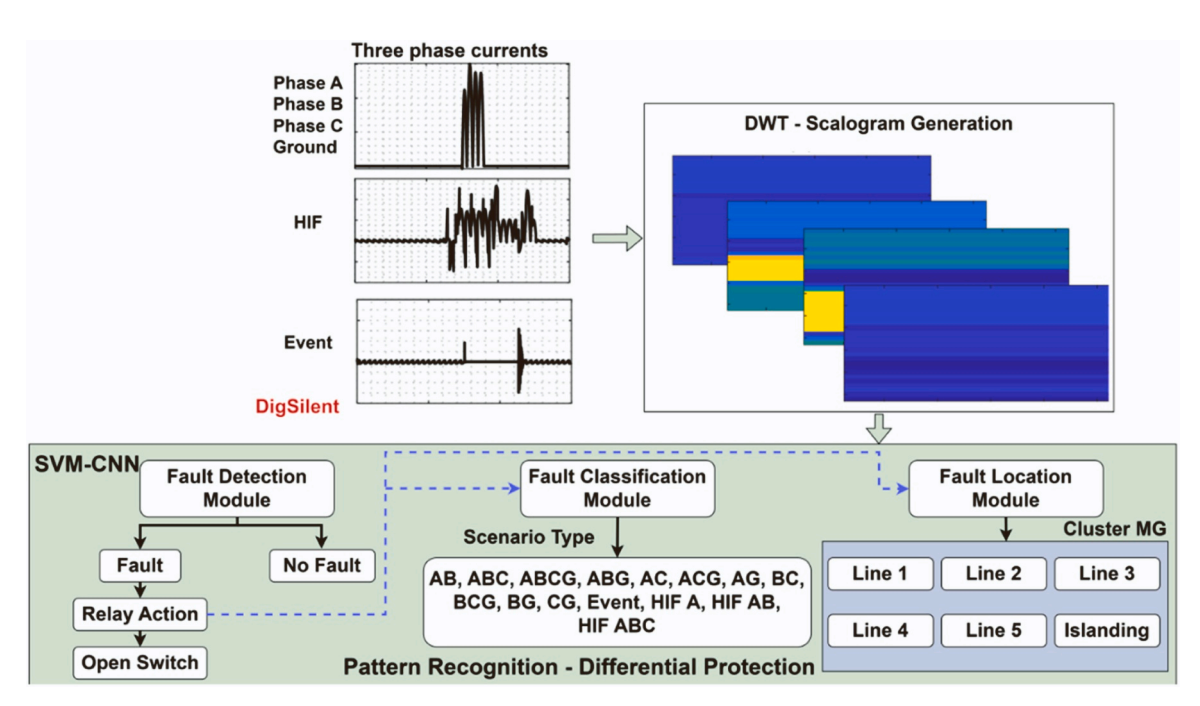


Fig. 1. Schematic representation of the proposed research.

calculated by Eq. (3) [32]:

$$\int |f(t)|^2 dt = \sum_{k} |c_0(k)|^2 + \sum_{k} \sum_{i=0} |d_i(k)|^2$$
(3)

The DWT allows obtaining optimal features for different frequency ranges in fault detection and localization studies in MGs. It is crucial to select the appropriate Wavelet to acquire accurate data. For datasets with a large number of samples, Daubechies wavelets (Db) and Symlets (Sym) Wavelets are often used due to their robustness and sample length.

2.2. Mathematical model and calibration of CNN

In data analysis, CNNs are employed for both multidimensional and one-dimensional data. Furthermore, in [33] the authors examine alternative algorithms for clustering and classifying real-time signals. CNNs excel in extracting features and classifying raw data, making them highly valuable for various applications. Researchers have demonstrated the effectiveness of CNNs in both small and large-scale data scenarios, yielding excellent results. CNNs operate by processing images through multiple layers, effectively isolating their distinctive features [34]. The most frequently utilized layers include:

2.2.1. Convolutional layer

This layer determines the features of the image. The number of convolutional layers is a crucial parameter for determining features, which increases as the features grow. CNN relies on the convolutional layer, and its operation is mathematically modeled by the following Eq. (4) [34].

$$R(x,y) = \sum_{i=1}^{k} \sum_{j=1}^{p} M(i,j) * A(x+1,y+j)$$
 (4)

where A is the feature matrix, and M is the mask, x and y are the row and column of the feature matrix, j and i are the column and row of the mask, and p and k are the column and row of the filter size, respectively.

2.2.2. Rectified linear unit layer (ReLU)

The activation layer of the system extensively utilizes non-linear functions due to their ability to process information swiftly. This is calculated using Eq. (5), allowing for efficient computation and enhanced model performance. The Rectified Linear Unit (ReLU) is particularly favored for its simplicity and effectiveness in neural networks, contributing to improved feature extraction and model robustness [28].

$$R(x,y) = \begin{cases} x & x \ge 0 \\ 0 & x < 0 \end{cases} \tag{5}$$

2.2.3. Pool layer

The Pooling Layer plays a crucial role in neural networks by down-sampling feature maps, effectively reducing computational load while retaining essential input properties. This process helps in managing model complexity and improving computational efficiency during training. By aggregating information from neighboring regions, the Pooling Layer enhances the network's ability to extract meaningful features and improves robustness against variations in input data [26].

2.2.4. Flatten layer

The data obtained from Section 2.1.3, represented in matrix form, is fitted to the fully connected (FC) layer. This strategic integration enables an expansion in the number of filters within the convolutional layers while mitigating the computational load. By effectively linking the convolutional outputs, the FC layer facilitates comprehensive feature extraction and enhances model capacity. The formulation for this layer's operation is articulated in Eq. (6), defining its pivotal role in neural

network architecture for optimizing performance [35]:

$$y_{ij}^{k} = \max \left(x_{ij}^{k'} : i \le i' < i + h, j \le j' < j + q \right)$$
(6)

where i,j are the elements of the k_{th} output and input feature maps, respectivel, q and h are the width and length of the pooling window, respectively.

2.2.5. Fully connected layer

The flattening layer is at the core of the neural network [36]. It extracts data, facilitating the learning process during neural network training. CNNs rely on hyperparameters that require optimization for configuring the network and enhancing learning parameters, enabling adaptation to large datasets. The three primary layers of CNNs—convolutional, pooling, and fully connected (FC)—are instrumental in optimizing these hyperparameters to achieve lower error rates and improved performance. Specifically, the convolutional operation optimizes six key hyperparameters: the number of feature maps and convolutional layers, their respective sizes, padding size, and stride. These parameters dictate how data is processed, facilitating feature extraction and the creation of feature maps [26], [32].

2.3. SVM mathematic modeling

Support vector machine is a supervised learning algorithm that divides two sets of data using a hyperplane, identifying the one that provides the largest margin between them. This approach enhances the classification confidence by maximizing the distance between the data points of different classes. SVM is widely used in signal processing problems, including the detection of electrical faults. It utilizes a Kernel function to classify and sample the data [33], a method further refined by [37]. The algorithm is versatile, allowing for application to multiclass and nonlinear datasets. Typically, among the many possible hyperplanes, the one with the greatest margin is selected to optimize classification accuracy. The SVM function is mathematically represented in Eq. (7) [38]:

$$f(x) = w^T \emptyset(x) + b \tag{7}$$

where $w \in \mathbb{R}^n$ and $\emptyset(x)$ is a feature map.

2.4. Proposed method

This study presents a method that combines CNN with a SVM algorithm to enhance classification performance. The approach involves initially training the CNN and then integrating the SVM for further refinement. Initially, the CNN is fully trained, after which the fully connected layer (FC-8) is removed. This process extracts features with dimensions of 4096 by the number of images in the dataset. These extracted features are then split, with 30 % allocated for training and 70 % for testing. The training features are then used to train an SVM classifier using a Gaussian kernel function and a one-vs-all classification method. The trained SVM classifier is subsequently employed to classify the testing features.

The process is repeated, this time by removing the maximum pooling layer (MaxPooling 7) from the CNN architecture. Despite potential concerns regarding overfitting due to the reduced number of parameters in the convolutional layers, the removal of the layer does not significantly impact the model's performance. Fig. 2 illustrates the modified scheme that incorporates the SVM algorithm into the CNN architecture, showcasing the integration and workflow of the combined approach. It is important to mention that before training the SVM-CNN model, the dataset underwent preprocessing steps to improve data quality and reduce noise. Specifically, we applied a smoothing technique using "smoothdata" in MATLAB to mitigate high-frequency noise while preserving underlying trends. Additionally, "medfilt1" was employed to

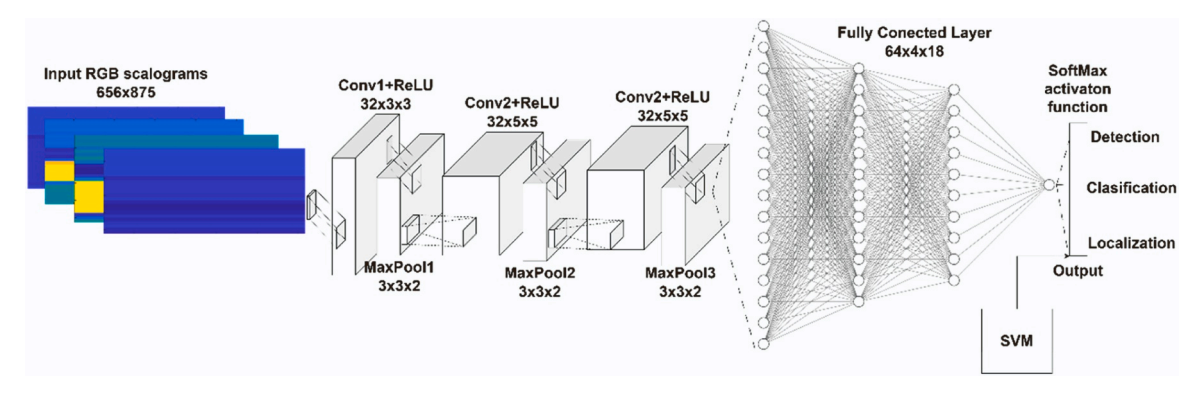


Fig. 2. Combination and adjustment of SVM-CNN architecture.

further smooth the dataset, ensuring robustness against outliers and spikes. These preprocessing steps were essential to ensure the reliability and accuracy of our results by minimizing potential errors during model training.

3. Case of study

In this article, a study and simulation were conducted on a MGC connected to the main grid, as illustrated in Fig. 3. Zones 1–3 comprise the MGC, while Zone 4 represents the external grid (outside the MGC). The main characteristics of the sources and loads forming each MG are detailed in Table 1A (Annexes). Lines L1 to L5 are analyzed using both differential protection and the proposed SVM-CNN method, with Zone D representing an external fault to the MGC. A total of 11 types of faults (AB, ABC, ABCG, ABG, AC, ACG, AG, BC, BCG, BG, CG) were analyzed, along with simulations of line opening and closing events, high-

impedance faults (HIF A, HIF AB, HIF ABC), and islanding mode. To collect more data and improve accuracy, resistances were varied for the 11 types of faults, islanding events, and line events (R=0.001 Ohm to 20 Ohm with variable steps; Table 2 A (Annexes) details the input data for SVM-CNN by varying fault type and fault resistance).

To evaluate the proposed model, a computational workstation equipped with an Intel Core i9 CPU running at 3.90 GHz and 16 GB of RAM, along with an NVIDIA GeForce RTX 3070 GPU, was used. The implementation of the SVM-CNN code was performed using MATLAB®, and real-time tests were conducted on Opal RT.

3.1. Calculation of the differential current

Fig. 4 illustrates the calculation of the differential current (ID) for the differential relay under various fault and event conditions in one of the lines of the MG cluster. The results encompass the characterization of

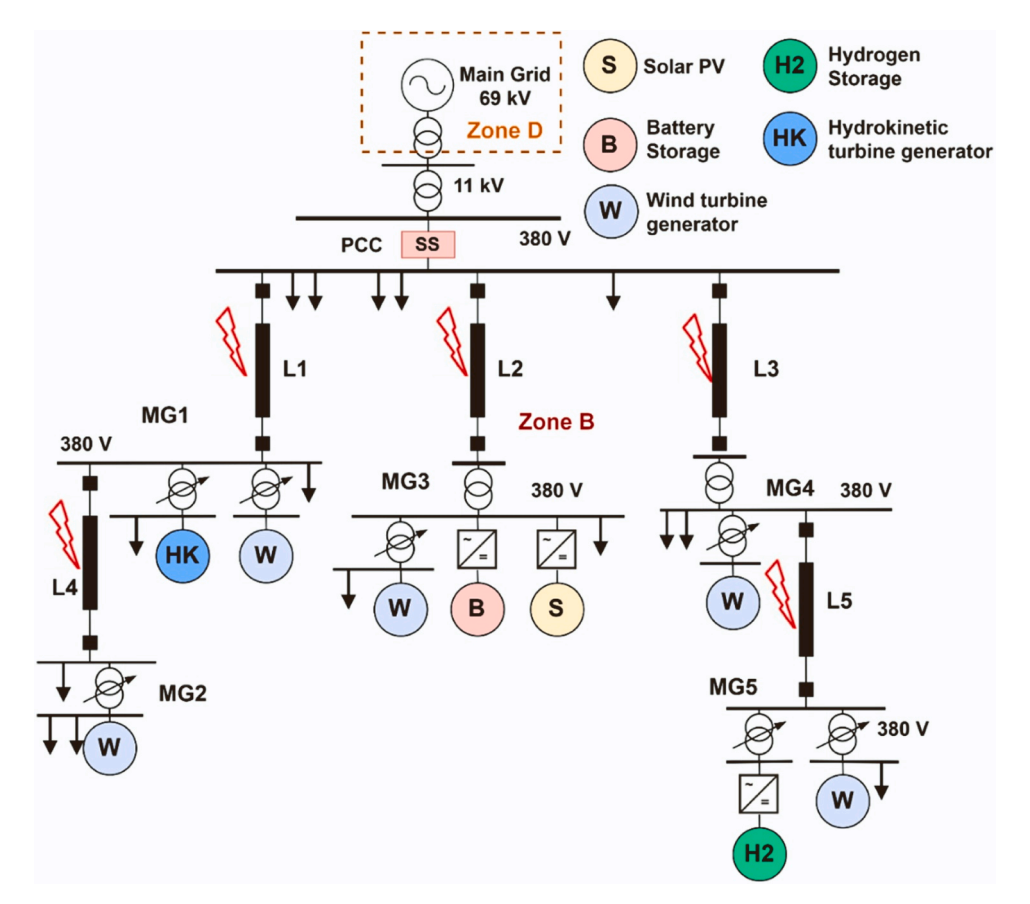


Fig. 3. Schematic representation of the studied MG cluster.

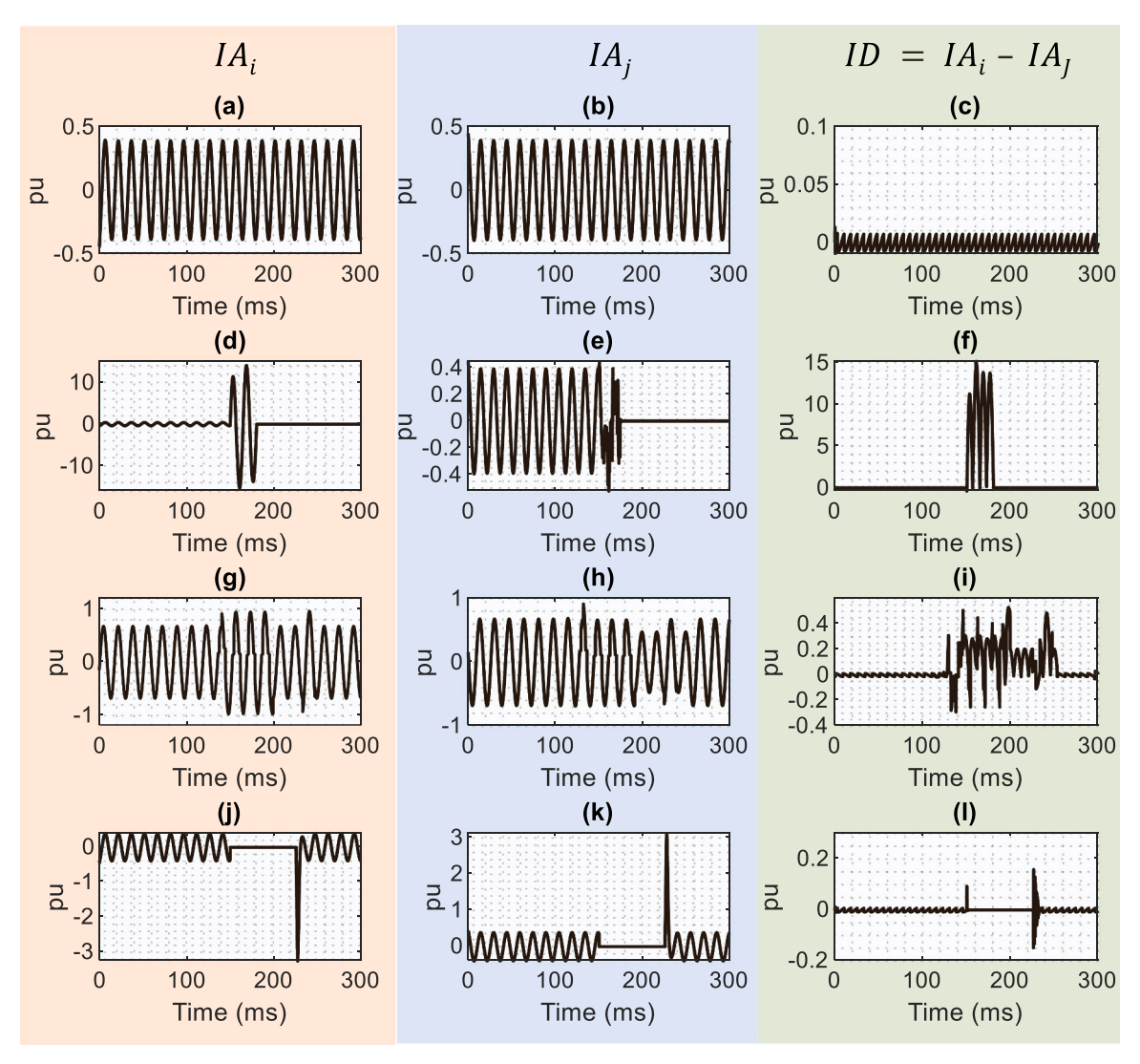


Fig. 4. Calculation of the differential current in phase A. (a), (b), and (c) depict nominal operating conditions. (d), (e), and (f) represent a ground fault. (g), (h), and (i) illustrate HIF. (j), (k), and (l) represent a transmission line opening and closing event.

the ID, crucial for fault detection and localization, with $ID=IA_i-IA_j$, where IA_i and IA_j represent the currents at the ends of the transmission line. This analysis was conducted across a range of operational scenarios to capture the complexity of electrical systems under both normal and contingency conditions. Initially, the system's normal operating condition was examined, providing a baseline reference for comparing ID variations in abnormal situations. Subsequently, a single-phase ground fault was simulated, a common event in distribution networks that can lead to significant current imbalances. Furthermore, the impact of a HIF was analyzed, which poses additional challenges for detection due to its transient and low-current nature. Then, the effects of transmission line opening and closing events were evaluated, considering abrupt changes in the system's topology. The results obtained provide input variables for the SVM-CNN algorithm tasked with recognizing the fault type based on the differential current ID.

3.2. DWT signal processing analysis

The results displayed in Fig. 5 present the transformation of the ID into the frequency domain through the DWT. Specifically, the WAC has been employed for this analysis. WAC demonstrates a notable divergence particularly during faults or anomalies, enhancing the differential protection system's ability to discern such occurrences more effectively.

Fig. 5 showcases various scenarios: Panels (a) and (e) exhibit the differential current and its corresponding WAC coefficient under normal operating conditions. Panels (b) and (f) depict a ground fault, while (c) and (g) demonstrate a HIF. Finally, panels (d) and (h) illustrate a transmission line opening and closing event.

Furthermore, Fig. 6 presents temporal and frequency domain representations of various fault types. Under normal conditions, panels (a) and (e) serve as baseline references, displaying temporal waveforms and scalograms respectively. During ground faults, panels (b) and (f) show characteristic variations in temporal and frequency domains. High impedance faults are depicted in panels (c) and (g), highlighting their unique temporal and frequency signatures. Panels (d) and (h) illustrate the effects of transmission line opening and closing events on signal characteristics. These insights are crucial for training CNN models to develop robust fault detection algorithms that utilize both temporal and frequency data.

Moreover, Fig. 7 illustrates the WAC for various single-phase ground fault resistances. It highlights that even for a ground fault resistance (Rg) as low as 20 Ohms, the WAC value surpasses that of a transmission line opening and closing event, as shown in Fig. 7(d) and Fig. 7(h). This comparison underscores the critical role of WAC in fault detection by revealing substantial differences in signal characteristics across different fault types. As fault resistance increases, traditional fault detection

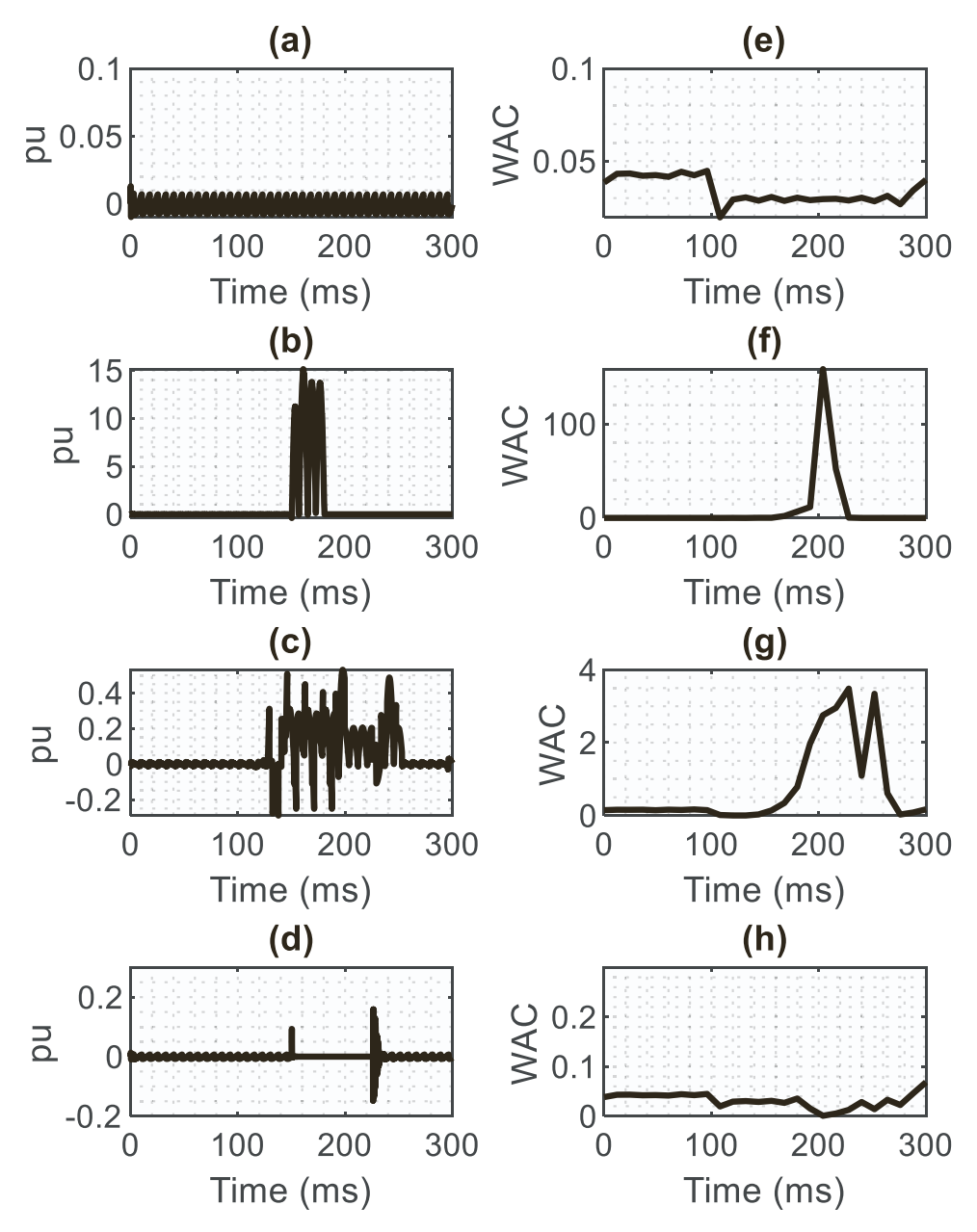


Fig. 5. Signal Processing on Line 2 for Phase A. (a) and (e) depict the differential current and its corresponding WAC under normal conditions. (b) and (f) represent a ground fault, while (c) and (g) illustrate a HIF. (d) and (h) demonstrate a transmission line opening and closing event.

methods encounter increasing challenges. Therefore, the integration of SVM-CNN becomes crucial for ensuring accurate fault detection in such scenarios.

3.3. Real-time testing configuration using OPAL-RT

The fault simulation tests were performed using the OPAL-RT real-time simulator, where various types of faults were simulated using models developed in Simulink/MATLAB® and validated on the RT-LAB platform. This configuration allowed for fine-tuning the method parameters to validate the results. Fig. 8 depicts the equipment utilized in this setup, which integrates the OPAL-RT real-time simulator connected via LAN to the Local Host. The simulation program operates under a Fixed-Step discretized method with an operating system utilizing Ts 50 μs and a switching frequency of 20 kHz. These specifications ensure reliable operation within a real-time environment, facilitating accurate and precise fault analysis and validation.

4. Results

4.1. Comparative analysis of signal decomposition techniques for fault detection

In Fig. 9, comparisons between the detail and approximation coefficients obtained through DWT are illustrated. Fig. 9(a) showcases DWT with detail coefficients, while Fig. 9(b) presents DWT with approximation coefficients. Additionally, Fig. 9(c) demonstrates the decomposition using WPT, and Fig. 9(d) exposes the VMD technique combined with the HT, revealing up to 20 IMF. This analysis is conducted with the aim of identifying the most prominent coefficients in simulated fault scenarios, specifically during a single-phase ground fault. The pursuit of the highest coefficient aims to facilitate fault detection while varying the fault resistance. In this context, preference is given to DWT approximation coefficients, owing to their ability to effectively highlight and classify faults, particularly in the presence of high fault resistances.

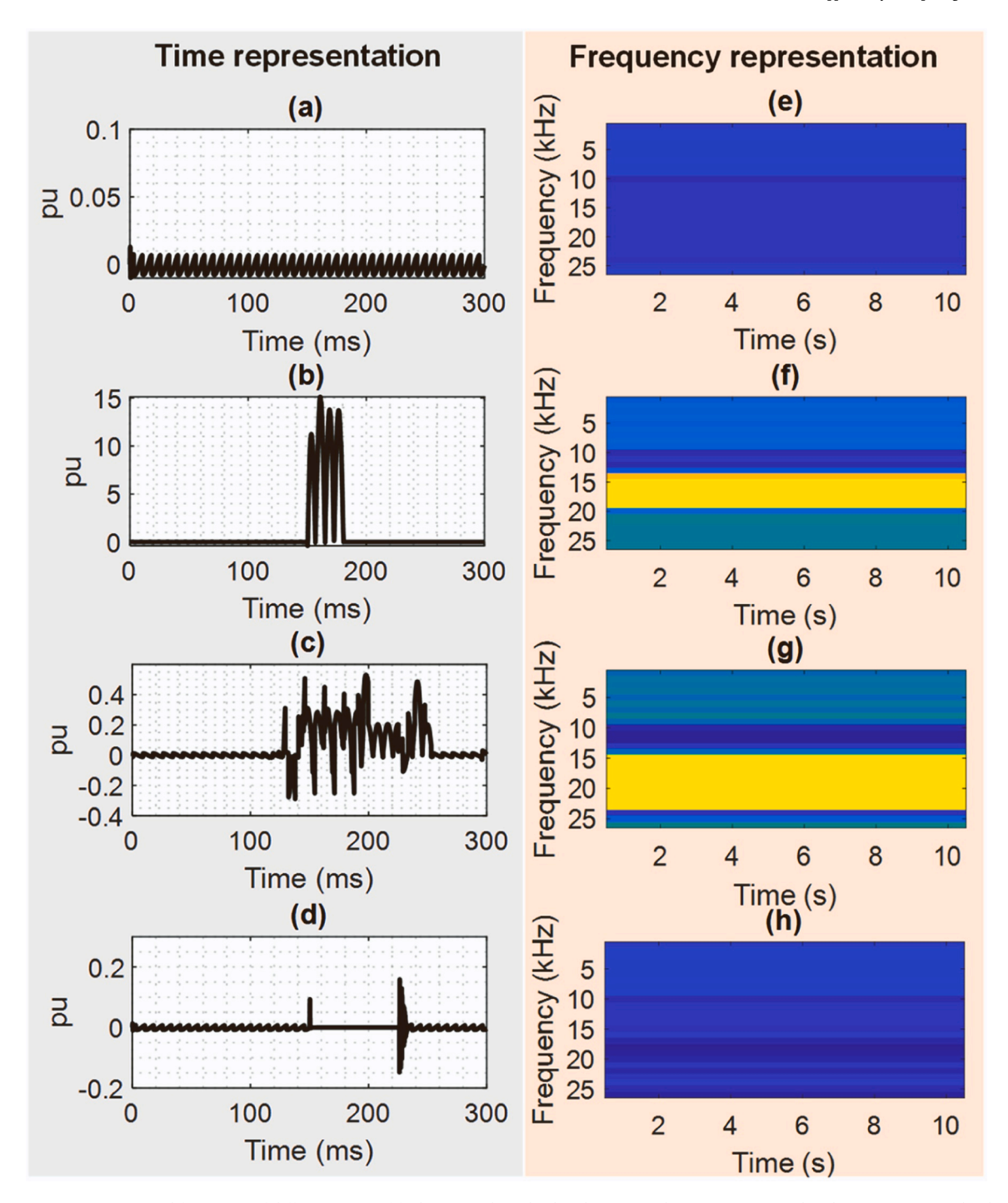


Fig. 6. Representation in time and frequency of different types of faults. (a) and (e) display the temporal representation and scalogram, respectively, during normal operation. (b) and (f) depict a ground fault, while (c) and (g) represent a HIF and (d) and (h) illustrate a transmission line opening and closing event.

The choice of using approximation coefficients from DWT at level 8 with the db6 base function, which reaches a maximum value of 163.18, is justified by their higher magnitude in fault scenarios. Similarly, the maximum detail coefficient obtained at level 9 with the db2 base function, reaching 106.30, reinforces this selection. Furthermore, the consideration of detail coefficients with a ground resistance of 0.001 Ohms adds to the robustness of the classification approach. These coefficients are selected for their effectiveness in fault detection, particularly in scenarios with high fault resistances, where they provide superior classification capabilities.

4.2. Performance and accuracy analysis of SVM-CNN

Fig. 10 depicts the result of the loss function value during the training of the proposed SVM-CNN model. The horizontal axis displays the number of epochs, while the vertical axis represents the value of the loss function. The curve begins at a high value and gradually decreases as the training progresses. The curve's shape suggests successful learning of the model. Initially, the curve starts at a high value because the model lacks knowledge of the data at the beginning of the training. As the training proceeds, the model learns from the data, leading to a decrease in the loss function. The curve is not perfectly smooth, indicating some noise in the data. However, the overall trend of the curve is downward,

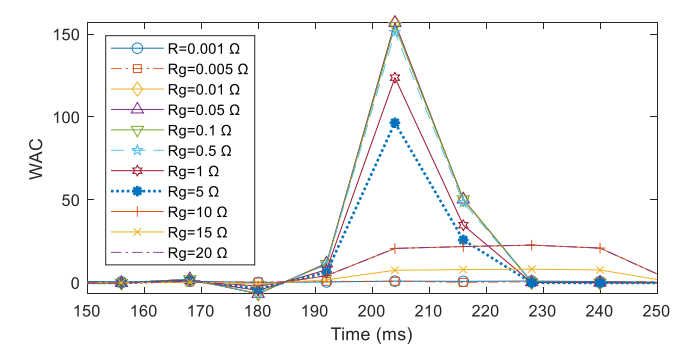


Fig. 7. Variation of WAC for various ground fault resistance values.

indicating successful learning of the model.

The value of the loss function on the training set, with the green line representing the value of the loss function on the validation set. The loss function value on the training set is always lower than that on the validation set because the model is trained to minimize the loss function on the training set. The difference between the loss function value on the training set and the loss function value on the validation set is called overfitting. Overfitting occurs when a model learns too much from the training data and does not generalize well to new data. In this case, the difference between the loss function value on the training set and the loss function value on the validation set is not significant, suggesting that the model is not overfitting. Overall, the proposed SVM-CNN model is successfully learning and is not overfitting.

4.3. K-Fold validation

In the evaluation of a model designed for detecting and localizing electrical faults in MGC lines using differential protection application, Fig. 11 presents the obtained results. It shows various metrics and performance indicators crucial for assessing the model's effectiveness. In the study, the number of folds was varied to explore various training and testing configurations. The number of folds, representing the number of divisions made in the dataset for model training and evaluation, has been explored in values from 1 to 15. This variability in the number of folds allows examining the model's robustness in different dataset partitioning scenarios. Evaluation metrics include Accuracy, F1-Score, Recall, and Matthews Correlation. Accuracy provides an overview of the model's precision, while the F1-Score offers a balanced measure between precision and the ability to correctly recover faults. Recall

measures the model's ability to identify all instances of faults, while Matthews Correlation provides a robust evaluation, considering all four quadrants of the confusion matrix.

The results show generally high performance in all evaluated metrics as the number of folds increases. Accuracy, F1-Score, Recall, and Matthews Correlation tend to converge towards values close to unity, suggesting consistent effectiveness in detecting and localizing electrical faults. These results support the differential protection model's ability to provide a reliable solution in MGC environments, enhancing electrical fault detection and localization accurately.

4.4. Sensitivity analysis

Expanding on the preceding examination of CNN hyperparameters, the sensitivity analysis (Fig. 12) investigates the influence of key configuration elements on the CNN's performance in data classification. This exploration covers optimization algorithms, activation functions, pooling layer sizes, and stride values, providing insights into how these factors affect both accuracy and detection time. In terms of optimization algorithms, three widely used options were evaluated: Adam, RMSprop, and SGD. Adam demonstrated superior performance by achieving the highest accuracy of 99.99 %, while maintaining an efficient detection time of 5.5 ms. In comparison, RMSprop and SGD achieved slightly lower accuracies of 97.36 % and 95.03 %, respectively, with detection times of 7.8 ms and 9.5 ms.

Building on the analysis of CNN hyperparameters, this section delves into key factors that influence the model's performance in data classification tasks as shown in Fig. 13. Initially, three common activation functions were evaluated: ReLU, Sigmoid, and Hyperbolic Tangent (Tanh). ReLU and Sigmoid achieved high accuracies of 99.99 % and 99.7 %, respectively, with detection times of 5.5 ms and 5.3 ms. Tanh also performed well, achieving 99.8 % accuracy with a detection time of 7.4 ms. Furthermore, various sizes of pooling layers (2×2, 3×3, and 4×4) were tested. The 3×3 pooling layer achieved the highest accuracy at 99.99 %, while the 2×2 and 4×4 sizes achieved accuracies of 99.75 % and 99.999 %, respectively. Detection times varied slightly: 4.9 ms for 2×2, 5.5 ms for 3×3, and 8.8 ms for 4×4.

Additionally, different stride values (1, 2, and 3) in the pooling layers were analyzed. A stride of 1 achieved 99.87 % accuracy with a detection time of 7.6 ms, while strides of 2 and 3 achieved accuracies of 99.99 % and 98.56 %, with detection times of 5.5 ms and 6.9 ms, respectively. Moving to Fig. 13 (a), the analysis extended to four critical categories: dropout rate, initial learning rate, L2 regularization, and number of training epochs. Dropout rate analysis ranging from 0.1 to 0.9, identified

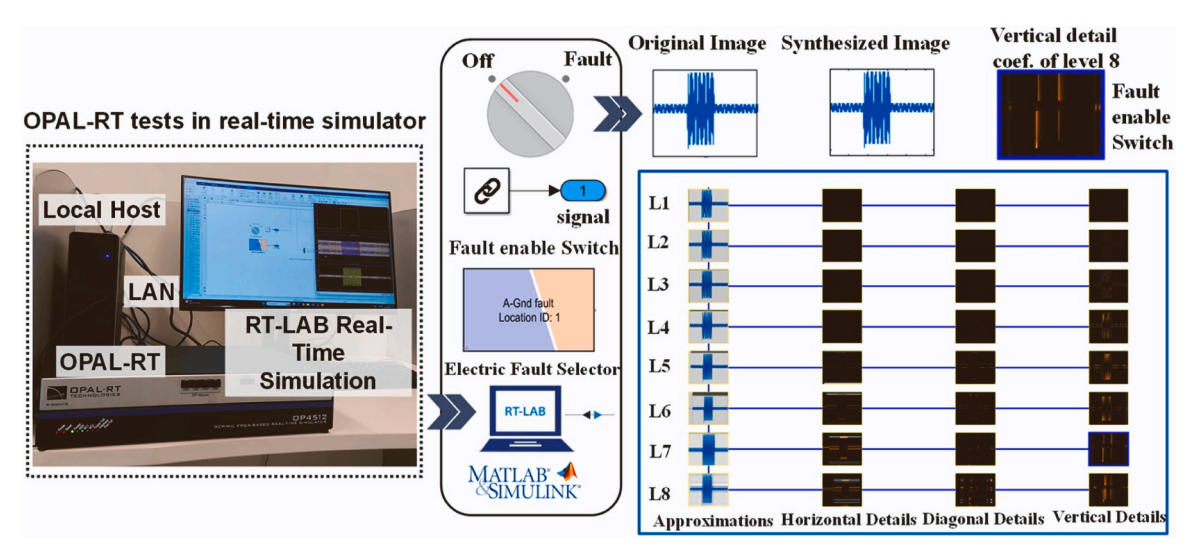


Fig. 8. Fault Simulation Case Study with RT-LAB Real-Time MATLAB®/Simulink.

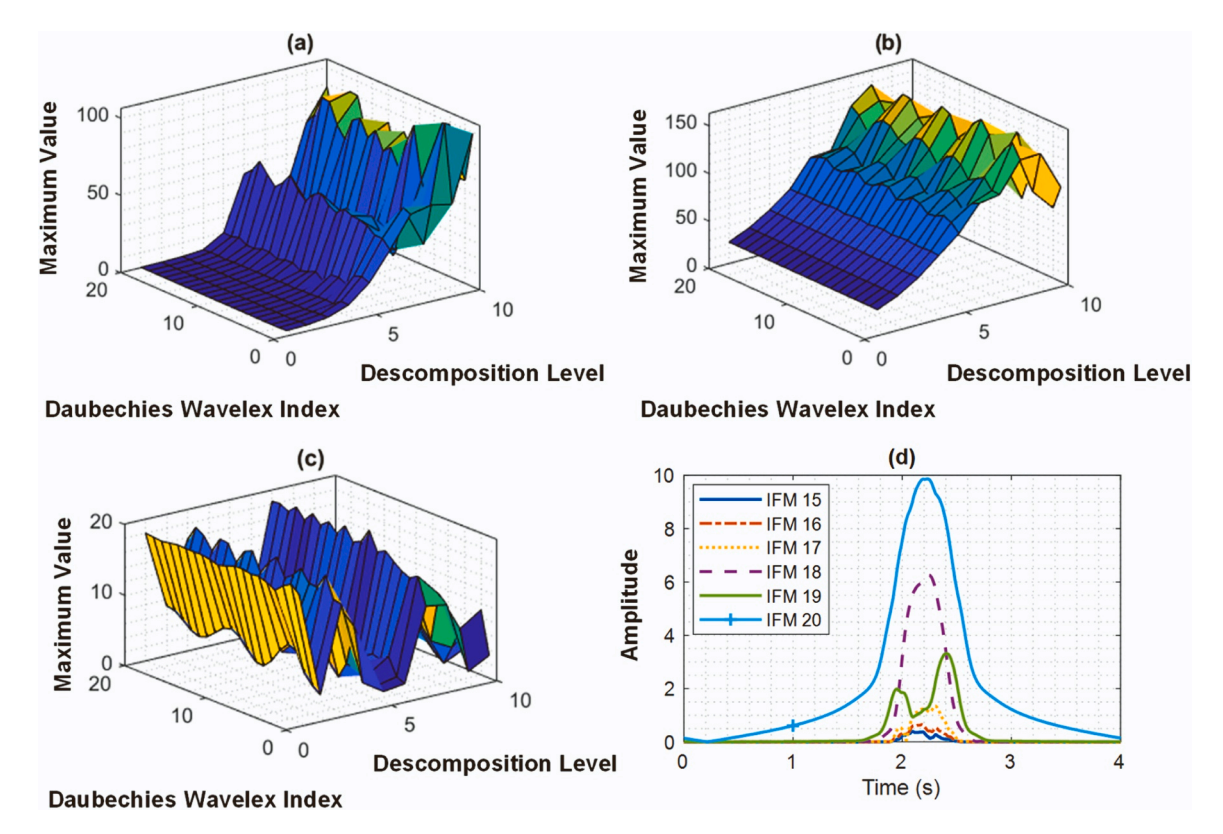
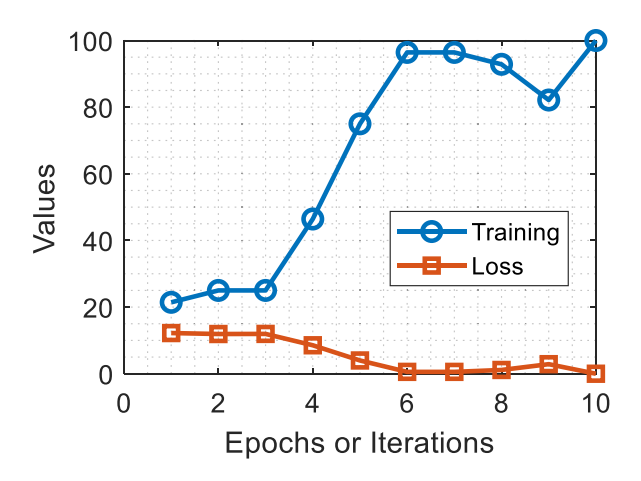


Fig. 9. Triphasic fault. (a) Detail Coefficients Maximum Values. (b) Approximation Coefficients Maximum Values. (c) Wavelet Packet Coefficients Maximum Values. (d) Hilbert Curves for Different Modes (Dominant frecuency bands).



 $\textbf{Fig. 10.} \ \ \textbf{Training and validation of the SVM-CNN Model.}$

an optimal balance at 0.5, achieving the highest accuracy of 99.999 %. Higher rates improved computational efficiency but reduced accuracy. In Fig. 13 (b), initial learning rates (ranging from 0.00001 to 0.1) showed optimal accuracy (99.99 %) at 0.00001, with higher rates maintaining high accuracy but requiring careful adjustment. L2 regularization shown in Fig. 13 (c), ranging from 0.00001 to 0.1, demonstrated optimal accuracy (99.99 %) at 0.00002, while higher values compromised accuracy due to increased regularization. Lastly, Fig. 13 (d) explored the impact of training epochs (10–5000), stabilizing accuracy at 99.99 % after 35 epochs, indicating convergence. Extended epochs increased training time, highlighting the balance needed between accuracy and computational efficiency.

4.5. Comparison with other methods

Table 1 presents a comprehensive comparison of various methods for detecting, classifying, and localizing electrical faults in a power system. Among traditional methods, the overcurrent relay exhibits an accuracy of 56 %, while the differential relay significantly improves with a 96 % accuracy. More advanced methods such as decision tree and random forest achieve accuracies of 97 % and 99 %, respectively, with specific classification capabilities. Neural network architectures, such as the 1-D CNN BiLSTM-Attention model and the Xception transformer, demonstrate accuracies of 94.53 % and 98.60 %, respectively, excelling in fault classification and localization across different phases and HIF. Other specialized approaches, such as WT-CNN, CNN-GTO, AI-CNN, and RFBNN, also offer high levels of accuracy in fault detection and classification, addressing specific parameters such as phases, switching events, and load changes. The proposed SVM-CNN method stands out as the most accurate with an accuracy of 100 %, achieving nearly perfect detection and classification of electrical faults. This comprehensive approach addresses specific parameters such as phases, HIF, switching events, and islanding.

4.6. Real-time simulation results with OPAL-RT

Fig. 14 presents the results obtained through the configuration on the RT-LAB platform, where the input step profile is analyzed in Fig. 14 (a), considering a phase-to-ground fault. In Fig. 14 (b) and 14 (c), disturbances in the voltage and current waveforms can be observed, respectively. A rapid system response is highlighted, with a recovery time of less than 10 ms after the fault occurrence. The three-phase voltage waveform in Fig. 14 (b) depicts sinusoidal curves for phases R, S, and T, each with identical frequency and amplitude but differing by 120 degrees in phase. The maximum amplitude of the sinusoidal curves is 1 per unit (pu), indicating a balanced three-phase system operating at a frequency of 50 Hz.

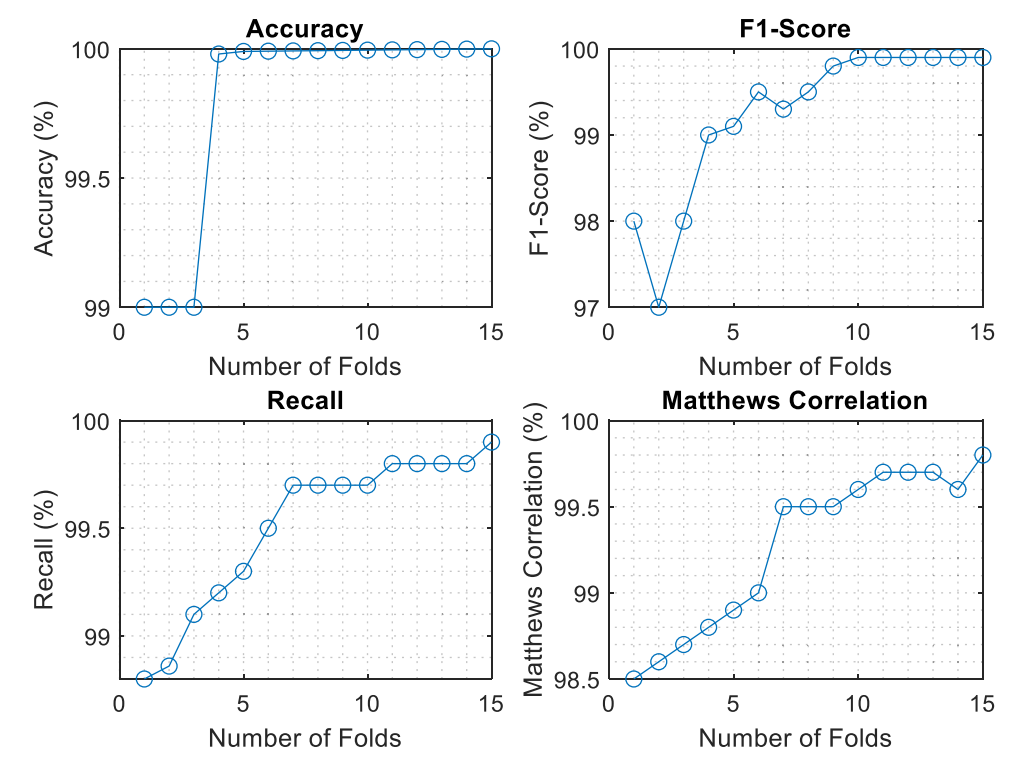


Fig. 11. K-Fold validation result.

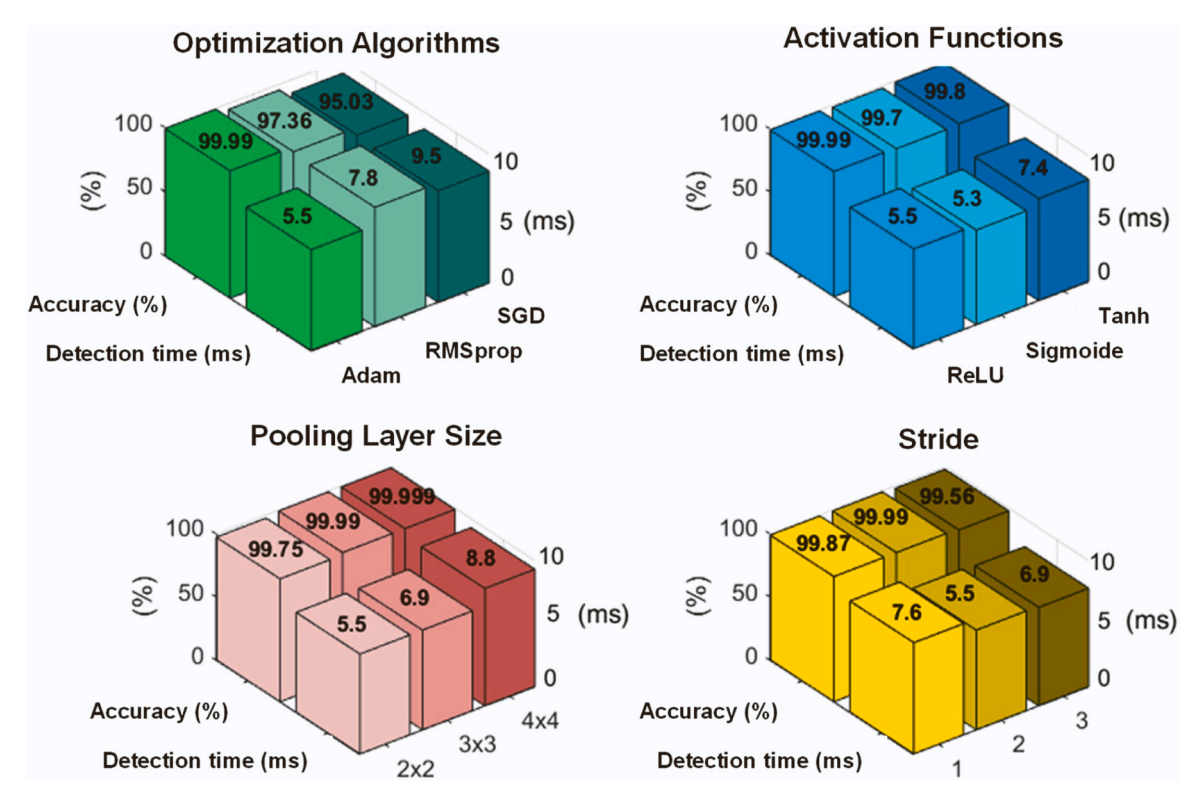


Fig. 12. Sensitivity analysis with respect to CNN parameters.

Similarly, Fig. 14 (c) illustrates the sinusoidal current intensities of phases R, S, and T over time, also at a frequency of 50 Hz with a maximum amplitude of 10 pu. This graph demonstrates the dynamic response of the electrical system, showing swift recovery of currents post-fault within a period of less than 10 ms. These findings underscore the effective performance of the RT-LAB platform for simulating and

analyzing critical events such as phase faults in three-phase systems, corroborating computer simulations conducted using DIgSILENT PowerFactory and MATLAB® in this study. The results provide a detailed evaluation of the stability and dynamic response of the electrical system, crucial for enhancing operational safety in industrial and power distribution environments.

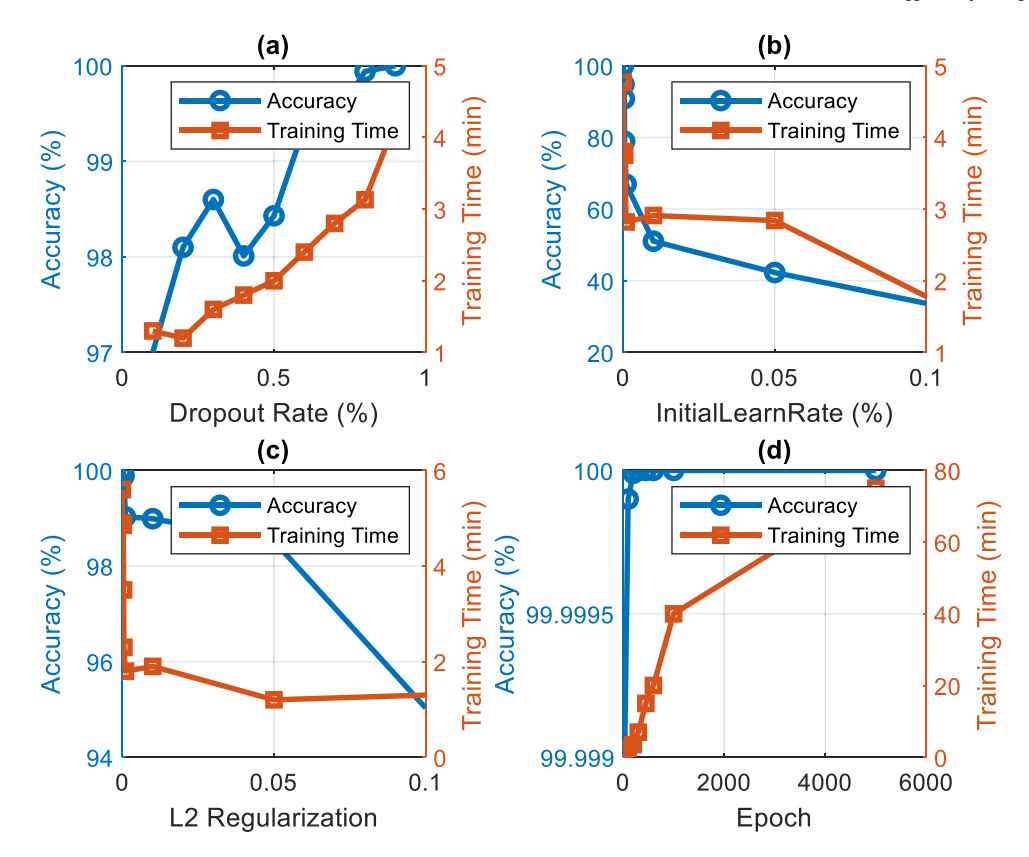


Fig. 13. Hyperparameter comparison for SVM-CNN model performance.

Table 1Comparative results with other methods.

Method	Accuracy (%	Parameter				
	Fault detection	Fault classification	Fault location	classification		
Over-current relay [27]	56.00	-	-	-		
Differencial relay [27]	96.00	-	-	-		
Decision Tree	97.00	85.00	-			
Random Forest	99.00	94.00	-			
SVM	92.05	91.03	90.85	Phases, HIF, switch event, islanding		
1-D CNN BiLSTM- Attention model	94.53	94.19	93.08	Phases		
Xception transformer [28]	98.60	98.60	98.60	Phases, HIF		
WT-CNN [26]	99.31	97.60	94.10	Phases, swith event		
CNN-GTO [29]	99.36	99.00	98.20	Phases		
AI-CNN [30]	99.95	99.95	_	HIF, load change		
RFBNN [30]	99.99	99.99	_	Phases		
SVM-CNN	100	99.99	99.99	Phases, HIF,		
proposed				switch event, islanding		

5. Conclusions

The importance of improving fault detection, classification, and localization in MGs due to the low fault current provided by renewable sources is highlighted. Through the proposal of a novel methodology

combining Support Vector Machine (SVM) and Convolutional Neural Network (CNN), these difficulties are addressed. The research reveals significant findings in electrical fault detection and classification. It was found that the maximum approximation coefficients of the DWT were reached at level 8 using the db6 base function, with a value of 163.18, while the maximum detail coefficients were recorded at level 9 with the db2 base function, reaching a value of 106.30. This supports the preference for DWT approximation coefficients due to their effective ability to highlight faults, even in high fault resistance scenarios.

The SVM-CNN model demonstrated successful learning with a gradual decrease in the loss function value during training, and the loss function on the training set was always lower than on the validation set, indicating effective learning without significant overfitting. Additionally, K-Fold analysis showed high performance in metrics such as accuracy, F1-Score, Recall, and Matthews Correlation, which converged to values close to unity as the number of folds increased.

Regarding sensitivity analysis, it was found that the Adam optimization algorithm achieved the highest accuracy of 99.99 %, with an efficient detection time of 5.5 ms. ReLU and Sigmoid activation functions also showed high accuracies with minimal detection times. Comparison with other methods highlighted that the proposed SVM-CNN method achieved the highest 100 % accuracy in fault detection and classification, surpassing others in precision and classification scope. Finally, in real-time simulation results using OPAL-RT, a controller response time of less than 10 ms after the occurrence of the fault was observed, underscoring the efficiency of the proposed methodology in fault detection and management.

To advance research in fault detection and classification in MG electrical systems, exploring new deep learning architectures such as recurrent neural networks or attention mechanisms could enhance the model's adaptability to dynamic data. Additionally, evaluating the scalability of the SVM-CNN model in larger and more complex electrical networks, and integrating additional data sources such as weather information, will strengthen predictive capabilities. Optimizing the model

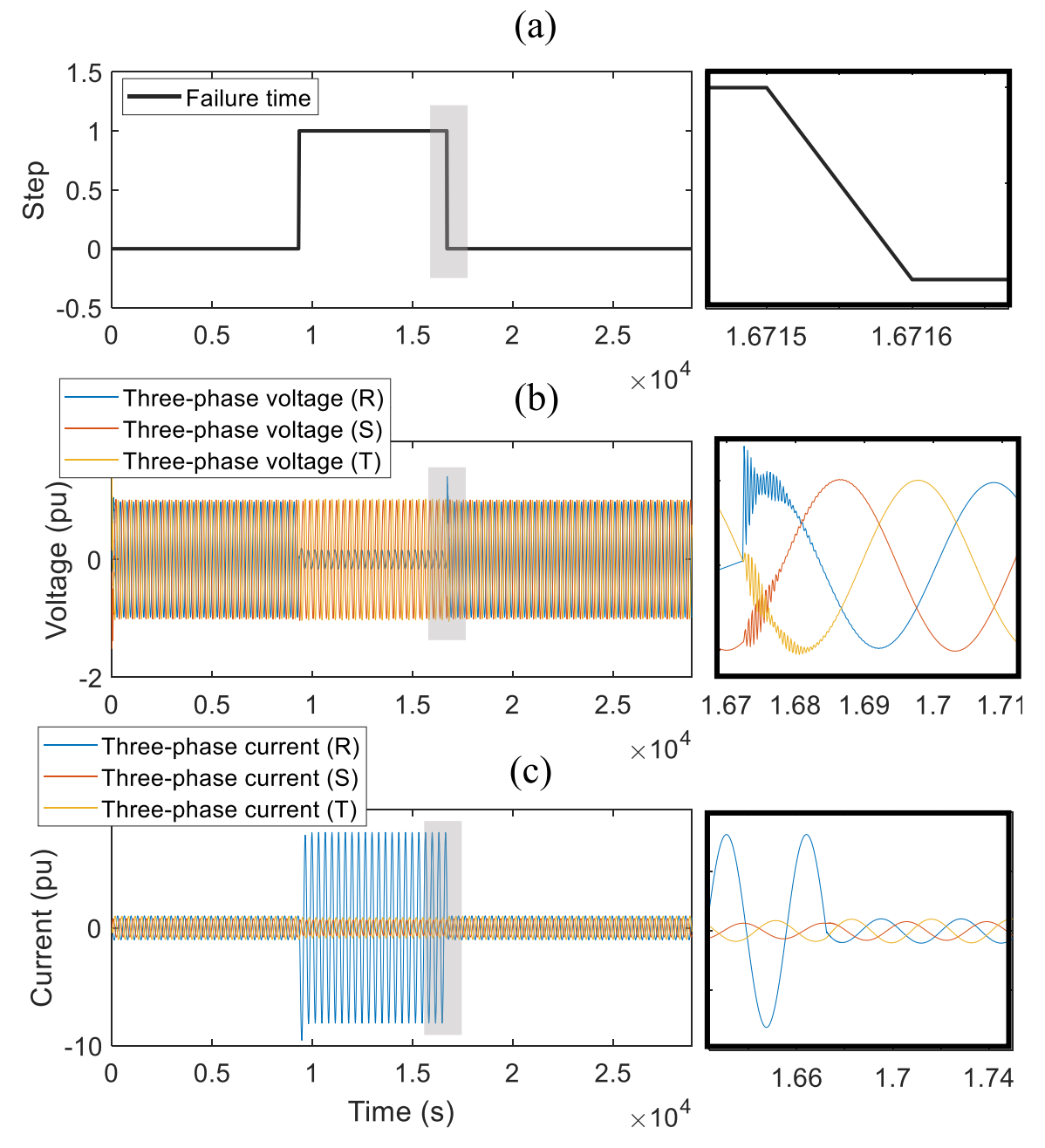


Fig. 14. Controller response in OPAL-RT real-time simulator: (a) Phase-to-ground fault simulation step. (b) Three-phase voltage measurement. (c) Three-phase current measurement.

for real-time implementation and conducting extensive experimental validations are also crucial steps to validate and refine its performance under real operating conditions of MGC.

CRediT authorship contribution statement

Antonio Cano: Software, Resources, Project administration, Methodology, Investigation. Paul Arévalo: Visualization, Validation, Supervision, Software, Resources, Project administration. Darío Benavides: Software, Resources, Project administration, Methodology, Investigation. Francisco Jurado: Methodology, Investigation, Funding acquisition, Formal analysis, Data curation, Conceptualization.

Declaration of Competing Interest

The authors declare that they have no known competing financial

interests or personal relationships that could have appeared to influence the work reported in this paper.

Data availability

Data will be made available on request.

Acknowledgment

The author (Paul Arévalo) thanks the Call for Grants for the Requalification of the Spanish University System for 2021–2023, Margarita Salas Grants for the training of young doctors awarded by the Ministry of Universities and financed by the European Union–Next Generation. The authors acknowledge the support provided by the Thematic Network 723RT0150 "Red para la integración a gran escala de energías renovables en sistemas eléctricos (RIBIERSE-CYTED)" financed by the call for

Thematic Networks of the CYTED (Ibero-American Program of Science

and Technology for Development) for 2022.

Annexes.

Table 1ADetails of MG cluster under study

MG	Source	Power (MW)	Power (MVA)	Load (MVA)
1	Wind	2.50	2.78	1.50
2	Wind, Hydrokinetic	9.10	12.78	8.34
3	Wind, Battery, PV	3.21	3.78	3.00
4	Wind	2.50	2.78	1.50
5	Wind, Hydrogen	2.62	3.08	2.00

Table 2A
Input and output parameters to the SVM-CNN model after data acquisition.

	Fault Gr. R.	Type of Fault	A	В	C	G	Α	В	С	G
No.			Input			Output				
1	R=0.001	ABC-G Fault	157.3769	163.0469	151.0852	8.1249	1	1	1	1
2	R=0.001	ABC Fault	158.3600	164.6300	152.6300	0.0000	1	1	1	0
3	R=0.001	AB-G Fault	163.5263	135.5837	0.2504	8.7753	1	1	0	1
4	R=0.001	AC-G Fault	131.9294	0.1003	152.2872	21.9378	1	0	1	1
5	R=0.001	BC-G Fault	0.1368	166.3500	129.2300	11.0429	0	1	1	1
6	R=0.001	A-B Fault	130.6827	132.0560	0.0740	0.0000	1	1	0	0
7	R=0.001	A-C Fault	135.1755	0.0977	134.0501	0.0000	1	0	1	0
8	R=0.001	B-C Fault	0.0612	131.2361	132.1972	0.0000	0	1	1	0
9	R=0.001	A-G Fault	142.5636	0.0977	0.0740	18.1980	1	0	0	1
10	R=0.001	B-G Fault	0.0577	140.0013	0.0740	12.7296	0	1	0	1
11	R=0.001	C-G Fault	0.0586	0.0977	131.3944	41.8812	0	0	1	1
12	R=0.001	No Fault	0.0447	0.0977	0.0838	0.0000	0	0	0	0
13	R=0.005	ABC-G Fault	156.9552	162.2815	150.7116	1.7856	1	1	1	1
14	R=0.005	ABC Fault	157.3700	163.0469	151.0862	0.0000	1	1	1	0
15	R=0.005	AB-G Fault	164.5163	135.3594	0.1900	1.8631	1	1	0	1
16	R=0.005	AC-G Fault	132.1304	0.1194	152.3109	4.5613	1	0	1	1
17	R=0.005	BC-G Fault	0.1668	166.9633	130.1749	2.2561	0	1	1	1
18	R=0.005	A-B Fault	130.6119	131.9554	0.0740	0.0000	1	1	0	0
19	R=0.005	A-C Fault	134.9908	0.0977	133.8721	0.0000	1	0	1	0
20	R=0.005	B-C Fault	0.0611	131.0771	132.0508	0.0000	0	1	1	0
21	R=0.005	A-G Fault	142.3151	0.0977	0.0740	3.8270	1	0	0	1
22	R=0.005	B-G Fault	0.0576	139.6938	0.0740	2.8880	0	1	0	1
23	R=0.005	C-G Fault	0.0587	0.0977	131.0947	9.0333	0	0	1	1
24	R=0.005	No Fault	0.0447	0.0977	0.0838	0.0000	0	0	0	0
25	R=0.01	ABC-G Fault	156.6826	161.8326	150.2581	0.0044	1	1	1	1
26	R=0.01	ABC Fault	156.9552	162.2815	150.7116	0.0000	1	1	1	0
129	R=20	A-G Fault	0.7997	0.0977	0.0761	0.0072	1	0	0	1
130	R=20	B-G Fault	0.0447	0.7549	0.0799	0.0101	0	1	0	1
131	R=20	C-G Fault	0.0447	0.0977	0.8055	0.0093	0	0	1	1
132	R=20	No Fault	0.0447	0.0977	0.0838	0.0000	0	0	0	0
132	Events	ABC	0.0447	0.0997	0.1230	0.0000	1	1	1	0
132	Events	A	0.0876	0.0977	0.0882	0.0000	1	0	0	0
132	Events	В	0.0664	0.2439	0.0818	0.0000	0	1	0	0
132	Events	C	0.0600	0.0977	0.0907	0.0000	0	0	1	0
	Type of Fault	HIF	A	В	C	G	Α	В	C	G
No.			Input				Outpu	ıt		
1	Phase	ABC	3.4824	3.4759	3.7459	0	1	1	1	0
2		AB	3.4824	3.4759	0.0838	0	1	1	0	0
3		AC	3.4824	0.0977	3.7459	0	1	0	1	0
4		BC	0.0447	3.4759	3.7459	0	0	1	1	0
5		A	3.4824	0.0977	0.0838	0	1	0	0	0
6		В	0.0447	3.4759	0.0838	0	0	1	0	0
7		С	0.0447	0.0977	3.7459	0	0	0	1	0

References

- A. Hooshyar, R. Iravani, Microgrid protection, Proc. IEEE 105 (2017) 1332–1353, https://doi.org/10.1109/JPROC.2017.2669342.
- [2] X. Liu, M. Shahidehpour, Z. Li, X. Liu, Y. Cao, Z. Bie, Microgrids for enhancing the power grid resilience in extreme conditions, IEEE Trans. Smart Grid 8 (2017) 589–597, https://doi.org/10.1109/TSG.2016.2579999.
- [3] L. Yan, M. Sheikholeslami, W. Gong, M. Shahidehpour, Z. Li, Architecture, control, and implementation of networked microgrids for future distribution systems, J. Mod. Power Syst. Clean. Energy 10 (2022) 286–299, https://doi.org/10.35833/MPCF.2021.000669
- [4] S.A. Arefifar, M. Ordonez, Y.A.R.I. Mohamed, Energy management in multimicrogrid systems - development and assessment, IEEE Trans. Power Syst. 32 (2017) 910–922, https://doi.org/10.1109/TPWRS.2016.2568858.
- [5] L. Meng, Q. Shafiee, G.F. Trecate, H. Karimi, D. Fulwani, X. Lu, J.M. Guerrero, Review on control of DC microgrids and multiple microgrid clusters, IEEE J. Emerg. Sel. Top. Power Electron 5 (2017) 928–948, https://doi.org/10.1109/ JESTPE.2017.2690219.
- [6] Y. Han, K. Zhang, H. Li, E.A.A. Coelho, J.M. Guerrero, MAS-based distributed coordinated control and optimization in microgrid and microgrid clusters: a comprehensive overview, IEEE Trans. Power Electron 33 (2018) 6488–6508, https://doi.org/10.1109/TPEL.2017.2761438.
- [7] M. Uzair, L. Li, M. Eskandari, J. Hossain, J.G. Zhu, Challenges, advances and future trends in AC microgrid protection: with a focus on intelligent learning methods, Renew. Sustain. Energy Rev. 178 (2023) 113228, https://doi.org/10.1016/J. RSFR 2023 113228
- [8] A.M. Entekhabi-Nooshabadi, H. Hashemi-Dezaki, S.A. Taher, Optimal microgrid's protection coordination considering N-1 contingency and optimum relay characteristics, Appl. Soft Comput. 98 (2021) 106741, https://doi.org/10.1016/J. ASOC 2020 106741
- [9] A. Azimi, H. Hashemi-Dezaki, Optimized protection coordination of microgrids considering power quality-based voltage indices incorporating optimal sizing and placement of fault current limiters, Sustain Cities Soc. 96 (2023) 104634, https:// doi.org/10.1016/J.SCS.2023.104634.
- [10] A.H. Ataee-Kachoee, H. Hashemi-Dezaki, A. Ketabi, Optimal adaptive protection of smart grids using high-set relays and smart selection of relay tripping characteristics considering different network configurations and operation modes, IET Gener., Transm. Distrib. 16 (2022) 5084–5116, https://doi.org/10.1049/ GTD2 12659
- [11] C. Reiz, J.B. Leite, Optimal coordination of protection devices in distribution networks with distributed energy resources and microgrids, IEEE Access 10 (2022) 99584–99594, https://doi.org/10.1109/ACCESS.2022.3203713.
- [12] Y.Y. Hong, M.T.A.M. Cabatac, Fault detection, classification, and location by static switch in microgrids using wavelet transform and taguchi-based artificial neural network, IEEE Syst. J. 14 (2020) 2725–2735, https://doi.org/10.1109/ ISYST 2019 2025504
- [13] A. Chandra, G.K. Singh, V. Pant, A novel high impedance fault detection strategy for microgrid based on differential energy signal of current signatures and entropy estimation, Electr. Power Compon. Syst. 52 (2024) 532–554, https://doi.org/ 10.1080/15325008.2023.2227193.
- [14] N. Bayati, E. Balouji, H.R. Baghaee, A. Hajizadeh, M. Soltani, Z. Lin, M. Savaghebi, Locating high-impedance faults in DC microgrid clusters using support vector machines, Appl. Energy 308 (2022) 118338, https://doi.org/10.1016/J. APENERGY.2021.118338.
- [15] P. Khandare, S.A. Deokar, A.M. Dixit, Optimization techniques using DWT-differentiation algorithms for fault detection and relay coordination in microgrid, Electr. Eng. 103 (2021) 493–503. (https://doi.org/10.1007/S00202-020-01089-1/FIGURES/8)
- [16] Fatemeh Mohammadi Shakiba, Artificial Neural Networks and Their Applications to Intelligent Fault Diagnosis of Power Transmission Lines | Guide books, New Jersey Institute of Technology, 2022. https://dl.acm.org/doi/10.5555/ AAI28971262 (accessed March 15, 2024).
- [17] M. Manohar, E. Koley, S. Ghosh, D.K. Mohanta, R.C. Bansal, Spatio-temporal information based protection scheme for PV integrated microgrid under solar irradiance intermittency using deep convolutional neural network, Int. J. Electr. Power Energy Syst. 116 (2020) 105576, https://doi.org/10.1016/J. JJEPES.2019.105576.

- [18] A. Pourfaraj, H. Iman-Eini, S. Bazyar, S. Ahmadi, E. Asadi, M. Langwasser, M. Liserre, A fault detection algorithm based on artificial neural network threshold selection in multi-terminal DC grids, IEEE Trans. Power Deliv. 38 (2023) 2510–2520, https://doi.org/10.1109/TPWRD.2023.3244853.
- [19] Y.Y. Hong, M.T.A.M. Cabatac, Fault detection, classification, and location by static switch in microgrids using wavelet transform and taguchi-based artificial neural network, IEEE Syst. J. 14 (2020) 2725–2735, https://doi.org/10.1109/ JSYST.2019.2925594.
- [20] M. Tripathy, Power transformer differential protection using neural network principal component analysis and radial basis function neural network, Simul. Model Pr. Theory 18 (2010) 600–611, https://doi.org/10.1016/J. SIMPAT.2010.01.003.
- [21] B.K. Chaitanya, A. Yadav, M. Pazoki, An improved differential protection scheme for micro-grid using time-frequency transform, Int. J. Electr. Power Energy Syst. 111 (2019) 132–143, https://doi.org/10.1016/J.IJEPES.2019.04.015.
- [22] A.H.N. Tajani, A. Bamshad, N. Ghaffarzadeh, A novel differential protection scheme for AC microgrids based on discrete wavelet transform, Electr. Power Syst. Res. 220 (2023) 109292, https://doi.org/10.1016/J.EPSR.2023.109292.
- [23] Y. Deng, S. Lin, L. Fu, K. Liao, L. Liu, Z. He, S. Gao, Y. Liu, New criterion of converter transformer differential protection based on wavelet energy entropy, IEEE Trans. Power Deliv. 34 (2019) 980–990, https://doi.org/10.1109/ TPWRD.2019.2893431.
- [24] D. Luo, T. Wu, M. Li, B. Yi, H. Zuo, Application of VMD and hilbert transform algorithms on detection of the ripple components of the DC signal, Page 935 13, Energies 2020 Vol. 13 (2020) 935, https://doi.org/10.3390/EN13040935.
- [25] Q. Li, X. Pang, D. Wang, Harmonic/inter-harmonic detection method based on variational mode decomposition and hilbert transform, 2023 IEEE 3rd Int. Conf. Electron. Technol., Commun. Inf., ICETCI 2023 (2023) 1411–1415, https://doi. org/10.1109/ICETCI57876.2023.10176872.
- [26] J.J.Q. Yu, Y. Hou, A.Y.S. Lam, V.O.K. Li, Intelligent fault detection scheme for microgrids with wavelet-based deep neural networks, IEEE Trans. Smart Grid 10 (2019) 1694–1703, https://doi.org/10.1109/TSG.2017.2776310.
- [27] D.P. Mishra, S.R. Samantaray, G. Joos, A combined wavelet and data-mining based intelligent protection scheme for microgrid, IEEE Trans. Smart Grid 7 (2016) 2295–2304, https://doi.org/10.1109/TSG.2015.2487501.
- [28] J.B. Thomas, S.G. Chaudhari, K.V. Shihabudheen, N.K. Verma, CNN-based transformer model for fault detection in power system networks, IEEE Trans. Instrum. Meas. 72 (2023), https://doi.org/10.1109/TIM.2023.3238059.
- [29] A.Y. Hatata, M.A. Essa, B.E. Sedhom, Adaptive protection scheme for FREEDM microgrid based on convolutional neural network and gorilla troops optimization technique, IEEE Access 10 (2022) 55583–55601, https://doi.org/10.1109/ACCESS.2022.3177544.
- [30] S. Wang, P. Dehghanian, On the use of artificial intelligence for high impedance fault detection and electrical safety, IEEE Trans. Ind. Appl. 56 (2020) 7208–7216, https://doi.org/10.1109/TIA.2020.3017698.
- [31] U.B. Baloglu, M. Talo, O. Yildirim, San Tan, R. Acharya, U.R. Classification of myocardial infarction with multi-lead ECG signals and deep CNN, Pattern Recognit. Lett. 122 (2019) 23–30.
- [32] H.K. Lee, Y.-S. Choi, Application of continuous wavelet transform and convolutional neural network in decoding motor imagery brain-computer interface, Entropy 21 (12) (2019) 1199.
- [33] Mallat, S.G. A Wavelet Tour of Signal Processing: The Sparse Way; Academic Press: New York, NY, USA, 2009.
- [34] A. Narin, Detection of focal and non-focal epileptic seizure using continuous wavelet transform-based scalogram images and pre-trained deep neural networks, IRBM Volume 43 (Issue 1) (February 2022) 22–31.
- [35] U.R. Acharya, H. Fujita, S.L. Oh, Y. Hagiwara, J.H. Tan, M. Adam, Application of deep convolutional neural network for automated detection of myocardial infarction using ECG signals, Inf. Sci. 415 (2017) 190–198.
- [36] J. Huang, B. Chen, B. Yao, W. He, ECG arrhythmia classification using STFT-based spectrogram and convolutional neural network, IEEE Access 7 (2019) 92871–92880.
- [37] M. Koklu, I.A. Ozkan, Multiclass classification of dry beans using computer vision and machine learning techniques, Comput. Electron Agric. 174 (2020) 105507.
- [38] C. Cortes, V. Vapnik, Support-vector networks, Mach. Learn 20 (3) (1995) 273–297.